The large-scale wall-to-wall interaction in fully developed turbulent channel flow

Y. S. Kwon[1], **K. Chauhan**[1], **C. M. de Silva**[1], **J. P. Monty**[1] **and N. Hutchins**[1]

[1]Department of Mechanical Engineering
The University of Melbourne, Victoria, 3010 AUSTRALIA

Abstract

The geometry of a high aspect ratio rectangular duct (channel) enforces symmetry in the mean flow. Instantaneously, however, large-scale motions on one side of the channel may influence the flow on the opposite side or cross over the symmetry plane itself. In this investigation, particle image velocimetry (PIV) is utilized to obtain two-component velocity fields in a streamwise-wall-normal plane over a very large area of a turbulent channel flow at a Reynolds number, $Re_\tau = hu_\tau/\nu \simeq 2100$ where h is the channel half-height, u_τ is the friction velocity and ν is the kinematic viscosity. Ensemble averages of fluctuating velocity fields conditioned on clockwise and counter-clockwise swirl events at the channel centreline reveal the presence of wall-to-wall interaction between large-scale motions.

Introduction

The geometry and boundary conditions in a turbulent channel flow ensure symmetry of the time-averaged turbulence statistics across the channel half-height. These statistics are conventionally studied over one half of the channel. However, instantaneous fluctuating velocity fields often show coherent large-scale, anti-symmetric features on either side of the centreline. In this paper, x denotes the streamwise coordinate and z denotes the wall-normal coordinate. Similarly, u denotes the streamwise velocity and w denotes the wall-normal velocity. The velocity quantities with a prime ($'$) indicate fluctuating components. For example, u' denotes the fluctuating streamwise velocity.

Dean and Bradshaw [3] considered turbulent channel flow as superposition of two boundary layers developing from both walls of the channel based on the results from conditional-sampling of hot-wire anemometry. Sabot and Comte-Bellot [6] observed burst-like patterns extending beyond the pipe centreline, which originate from flow structures associated with either sides of pipe wall, in turbulent pipe flows. Teitel and Antonia [7] used $u'w'$-quadrant analysis (note that we denote wall-normal velocity as w whereas Teitel and Antonia used v) to find that Q2 ($u' < 0, w' > 0$) events originating from one side of the channel can extend beyond the channel centreline. They also noted that the flow structures associated with opposite pair of channel walls are anti-symmetric about the centreline.

The above studies are based on measurements from hot-wire anemometry. In this investigation, we can access an extensive instantaneous velocity field through the use of PIV. One of the popular methodologies for identifying vortices in a two-dimensional (2D) vector field is by using *swirling strength*, λ_{ci} (see [9]). Swirling strength is the imaginary part of complex eigenvalue of the velocity gradient tensor, $\nabla \mathbf{u}$. Similar to vorticity, swirling strength is a measure of the strength of vortices. However, the effect of the strong shear layer is excluded in swirling strength unlike vorticity. Using linear stochastic estimation (LSE), based on swirl events near log region, Christensen and Adrian [2] showed organized vortices as evidence of hairpin vortex packets in turbulent channel flow while Hambleton *et al.* [4] looked at average flow fields in the streamwise-wall-normal and streamwise-spanwise
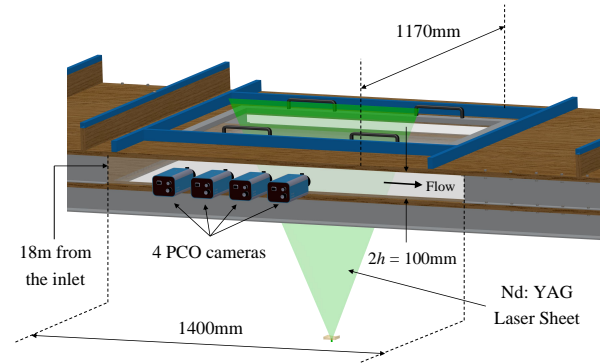

Figure 1: Experimental setup for 2D planar PIV.

plane around swirl events. Wu and Christensen [8] examined the population density and fraction of prograde (in the direction of mean vorticity) and retrograde (in the opposite direction of mean vorticity) vortices, which are identified using swirling strength, as a function of wall-normal position. They considered an interaction region, where flow structures originating from both walls co-exist, to be $\pm 0.55h$ from the channel centreline. In this interaction region, both population density and fraction of retrograde vortices for turbulent channel flow deviates from those for turbulent boundary layers, which is likely to be caused by the influence of the opposite wall. This study aims to understand the interaction of large-scale motions between the top and bottom walls via conditional averaging of velocity fields across the complete channel height for $Re_\tau = hu_\tau/\nu \simeq 2100$.

Experimental set-up

The experiments are conducted in the channel flow facility at the Walter Bassett Aerodynamics Laboratory located at the University of Melbourne. Details of the construction of the channel flow facility are provided in [5]. The facility is able to generate a maximum flow rate of approximately 3.6m^3/s, which equates to a bulk velocity of approximately 30m/s in the working section. The working section measures 22m in length with a cross section of 1170×100mm^2. A glass section was built into the existing facility, as shown in figure 1, to enable optical access, which is necessary for conducting the experiments. The modifications consisted of a glass floor and glass side walls with a length of 1400mm in the streamwise direction. The roof consisted of a removable glass section with a length of 500mm in the streamwise direction. The PIV measurements were conducted approximately 18m downstream of the inlet to the working section. This ensures that the flow is fully developed for the first and the second order statistics [5].

A two-dimensional planar PIV experiment was setup, as shown in figure 1, using four cameras placed horizontally. The streamwise (u) and wall-normal (w) velocity components were determined using a laser sheet in the streamwise-wall-normal plane.
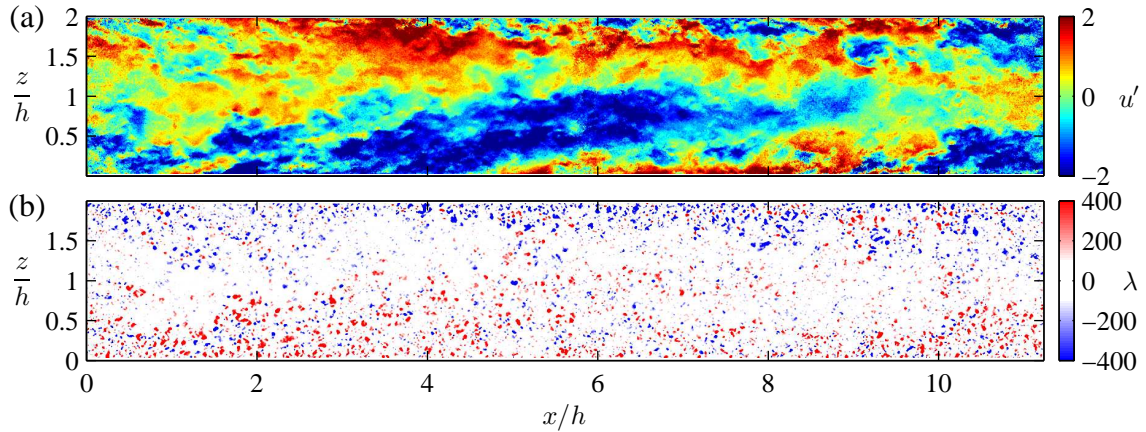
Figure 2: (a) Instantaneous streamwise velocity fluctuations in m/s and (b) Instantaneous signed swirl field, λ, in 1/s at the same instance for $Re_\tau \simeq 2100$.

Since multiple cameras were used, it was possible to obtain a large field of view of approximately 0.6m (12h) in the streamwise direction and the height of the channel (2h = 0.1m) in the wall-normal direction. An overlap region of approximately 4cm is used between cameras, and each camera provides velocity vectors up to the midpoint of this overlap region, enabling us to disregard 2cm from the edge of each image. Using a $36 \times 24mm^2$ sensor (PCO 4000 camera) with a resolution of 4008×2672 pixels and a 105mm Sigma macro lens enabled us to obtain a pixel size of approximately $45\mu m$. The laser source used was a dual cavity ND: YAG Big SKY laser (180mJ/pulse) with a wavelength of 532nm, which was passed through a series of lenses to generate a laser sheet. Spatial correlation was performed using a multigrid, multipass algorithm based on fast Fourier transforms developed in MATLAB. A final window size of 16×16 pixels was used for processing, which corresponds to a window size of $l^+ \simeq 30$ at $Re \simeq 2100$ where $l^+ = lu_\tau/\nu$.

Results

Figure 2(a) shows an example of a streamwise fluctuating velocity field over the full channel obtained from PIV. We can clearly see large-scale anti-symmetric momentum zones on either side of the centreline, extending over the streamwise distance of about 6h. To distinguish vortices with different orientations, signed swirling strength, λ, is obtained by multiplying λ_{ci} with the sign of spanwise vorticity as shown in equation 1, where ω_y denotes spanwise vorticity. Figure 2(b) shows λ at the same instance as the streamwise fluctuating velocity field in figure 2(a). Positive swirling events tend to align along the boundary of the low-speed region found in figure 2(a). This suggests that series of vortices align on top of an inclined low-speed region.

$$\lambda = \lambda_{ci} \frac{\omega_y}{|\omega_y|} \qquad (1)$$

In order to explore the wall-to-wall interaction of large-scale motions, ensemble averages of the flow fields are obtained, which are conditioned on occurrences of vortices at the channel centreline. Large-scale motions are detected by identifying vortices using the signed swirling strength, λ, since it is shown in figure 2 that swirling events are associated large-scale events. The speckle noise in swirling strength and vorticity fields is removed using a 3×3 median filter. Thereafter, streamwise fluctuating velocity fields are conditionally averaged based on the sign of the swirling strength at the reference wall-normal posi-

tions of $z = h$ and $z = 0.4h$. A total of 1210 PIV vector fields are used in the averaging. The number of fields available is effectively doubled by also including the same set of PIV vector fields, mirrored about the channel centreline.

Figure 3(a) shows contour plot of conditionally averaged streamwise velocity fluctuations, $u'^+ = u'/u_\tau$, based on positively signed swirling strength at the reference wall-normal position of $z = h$. Since the mirrored set of vector fields is also included in the analysis, contour plot of conditionally averaged u'^+ based on negatively signed swirling strength will simply be the mirror image of figure 3(a) about the channel centreline. This conditional averaged u'^+ contour plot reveals large-scale motions, which are anti-symmetric about the channel centreline. Vortices with positively signed swirling strength are associated with large-scale elongated low- and high-speed regions (figure 3a). Those high- and low- speed regions are attached on the top and bottom walls, respectively, and incline towards the condition point while extending for streamwise distances of more than 6h. This suggests that they originate from the top and bottom walls.

Directional fields for the fluctuating velocities are obtained by normalizing the magnitudes of all fluctuating velocity vectors to unity, similar to directional fields obtained from LSE found in [2] and [4]. LSE is a linear estimate of the conditional average such that the mean-square error between the conditional average and the estimate is minimum (see [1] for more details). The mathematical expression for LSE conditioned on positively signed swirling strength, λ_p is given in equation 2 where $\mathbf{x} = (x,z)$ is the condition point and $\mathbf{r}$ is the distance from $\mathbf{x}$.

$$\langle u'_j(\mathbf{x}+\mathbf{r})|\lambda_p(\mathbf{x})\rangle \approx \frac{\langle \lambda_p(\mathbf{x})u'_j(\mathbf{x}+\mathbf{r})\rangle}{\langle \lambda_p(\mathbf{x})\lambda_p(\mathbf{x})\rangle}\lambda_p(\mathbf{x}) \qquad (2)$$

The extent of large streamwise coherence is more apparent in the fluctuating directional fields. Figure 3(b) shows plots of fluctuating directional field over the contours of u'^+, conditionally averaged on positively signed swirl events at the reference wall-normal position of $z = h$. The directional field shows high- and low- speed regions extending for streamwise distances of more than 9h. Around vortices with positive vorticity (figure 3b), large-scale low- and high-speed regions extend on the bottom and top halves of the channel centreline. As compared to the contour plots of u'^+, the directional fields show the true extent of the coherent motions as they are less affected by the
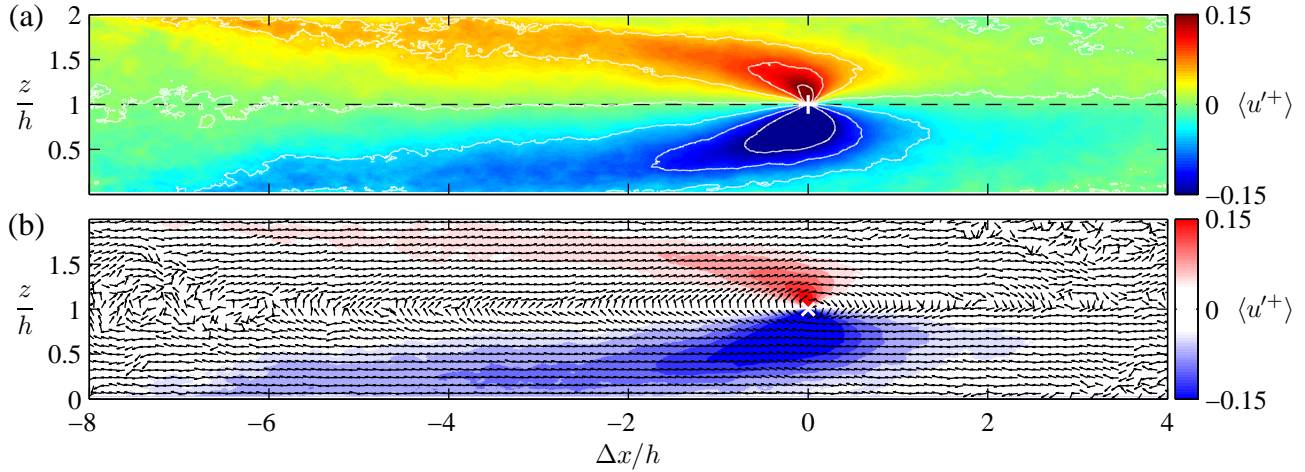
Figure 3: (a) Contour plot of u'^{+} and (b) fluctuating directional fields over contours of u'^{+}, conditionally averaged on positively signed swirl events at the reference position of $z = h$. Δx is the streamwise distance from the condition point. Black dashed line in (a) indicates channel centreline. White lines in (a) indicate line contours of u'^{+}, whose levels are from -0.15 to 0.15 in steps of 0.05. Contour levels indicate $\langle u'^{+} | \lambda > 0 \rangle$ for both (a) and (b). White '+' in (a) and '×' in (b) indicate the condition point.

low signal-to-noise ratio, which contaminates the flow fields far away from the condition points.

Figure 4 shows contour plots of conditionally averaged streamwise velocity fluctuations, u'^{+}, based on positively and negatively signed swirling strength at the reference wall-normal position of $z = 0.4h$ and figure 5 shows the corresponding fluctuating directional fields over the contours of u'^{+}. Here, the sign of the mean vorticity in the lower half of the channel is positive. Therefore, positive swirl events at $z = 0.4h$ indicate vortices rotating in the direction of the mean vorticity whereas negative swirl events at $z = 0.4h$ indicate vortices rotating against the mean vorticity.

Figure 4(a) shows that the negative swirl events at the reference wall-normal position of $z = 0.4h$ are flanked by high-speed region on the bottom and low-speed region on the top, both elongated in the streamwise direction. The coherence of those high- and low-speed regions can be seen in figure 5(a) more clearly. Also note that in figure 5(a), a pair of counter-rotating vortices is observed, which is consistent with observations from [4]. The centre of this clockwise vortex is located at the wall-normal position of about $z \simeq 1.1h$ and about $0.5h$ downstream of the counter-clockwise condition vortex at $z = 0.4h$ and $\Delta x = 0$.

In comparison, figure 4(b) shows that the positive swirl events at the reference wall-normal position of $z = 0.4h$ are flanked by low-speed region on the bottom and high-speed region on the top. Directional field in figure 5(b) shows the high- and low-speed region around positive swirl events are also elongated in the streamwise direction. The low-speed region under positive swirl events persists much further in the streamwise direction (order of $10h$) than the high- or low-speed region around negative swirl events. This is expected because the vortices with negatively signed swirling strength work against the mean vorticity in the channel, therefore, the structures associated with the vortices with negatively signed swirling strength cannot grow as much as that associated with the vortices with positively signed swirling strength.

Conditionally averaged directional field in figure 5(b) shows an inclined shear layer downstream of the condition point of positive swirl events. According to the hairpin vortex model, heads of vortices lie along this inclined shear layer with a long, low-speed region underneath the shear layer. Albeit being weak,

region of organized directional vectors above the large-scale, low-speed region implies that there is a region of coherent high-speed motions. This high-speed region does not extend as far downstream as the low-speed region but reaches almost to the opposite wall of the channel. The appearances of the clockwise vortex in figure 5(a) and the high-speed region in figure 5(b) show that even the vortices located closer to the wall ($z = 0.4h$) can influence the large-scale flow structures in the opposite wall. However, this influence due to vortices at $z = 0.4h$ is much weaker than that due to vortices at the channel centreline.

Conclusions

The nature of the wall-to-wall interaction of large-scale motions in turbulent channel flow is investigated by conditional averaging of a very large velocity field database. The conditional averages around vortices on the channel centreline reveal large-scale (of the order of $9h$), coherent high- and low-streamwise momentum zones, which are anti-symmetric about the channel centreline. This supports the hypothesis that channel flows can be conceptually considered as two interacting shear flows, originating from the top and bottom walls of the channel.

Vortices located nearer to the wall can also influence large-scale motions in the opposite half of the channel. The fluctuating flow fields, conditionally averaged on the vortices at a reference position of $z = 0.4$, show previously discovered flow features such as inclined low-momentum region, inclined shear layer and a pair of counter-rotating vortices. The weak, high-speed region is also observed above the large-scale low-momentum region. This high-speed region and the pair of counter-rotating vortices extend beyond the channel centreline on average, suggesting that the flow features associated with vortices at $z = 0.4h$ can also influence the large-scale motions in the opposite half of the channel. However this influence is weak and requires further investigation.

Overall, it is shown that flow structures originating from one half of channel can influence flow structures in the opposite half of channel, at least in the outer region of the flow. These anti-symmetric and large-scale motions are not only an artifact of the averaging process since they are also often found in instantaneous flow fields. The coherence of the anti-symmetric flow structures over a large streamwise domain, which is observed around vortices near the channel centreline, provides statisti-
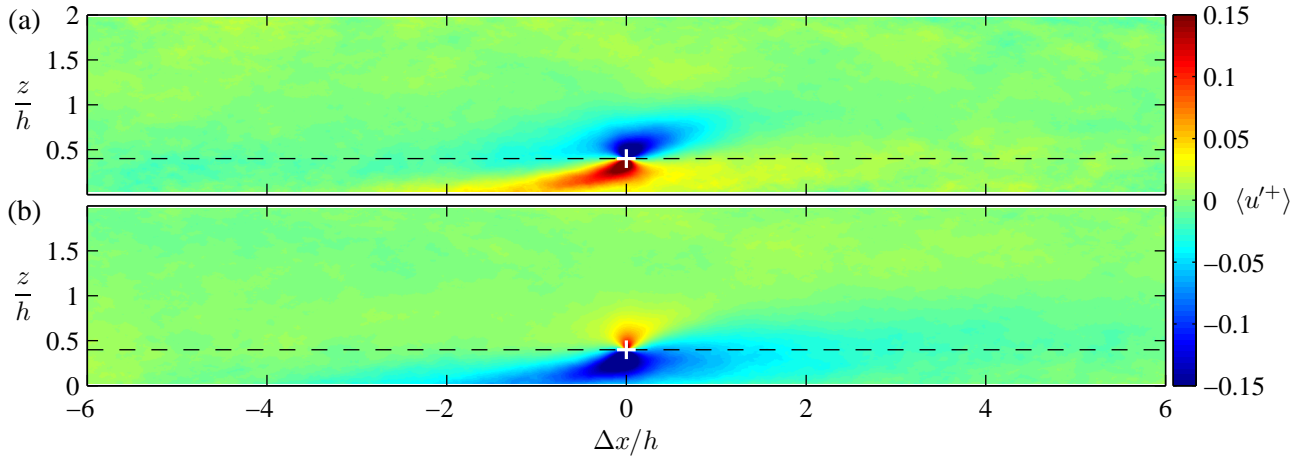
Figure 4: Contour plots of u'^+, conditionally averaged on (a) negatively signed and (b) positively signed swirl events at the reference position of $z = 0.4h$. Δx is the streamwise distance from the condition point. Black dashed lines indicate the reference wall-normal position of $z = 0.4h$. Contour levels indicate (a) $\langle u'^+|\lambda < 0 \rangle$ and (b) $\langle u'^+|\lambda > 0 \rangle$. White '+' indicates the condition points.
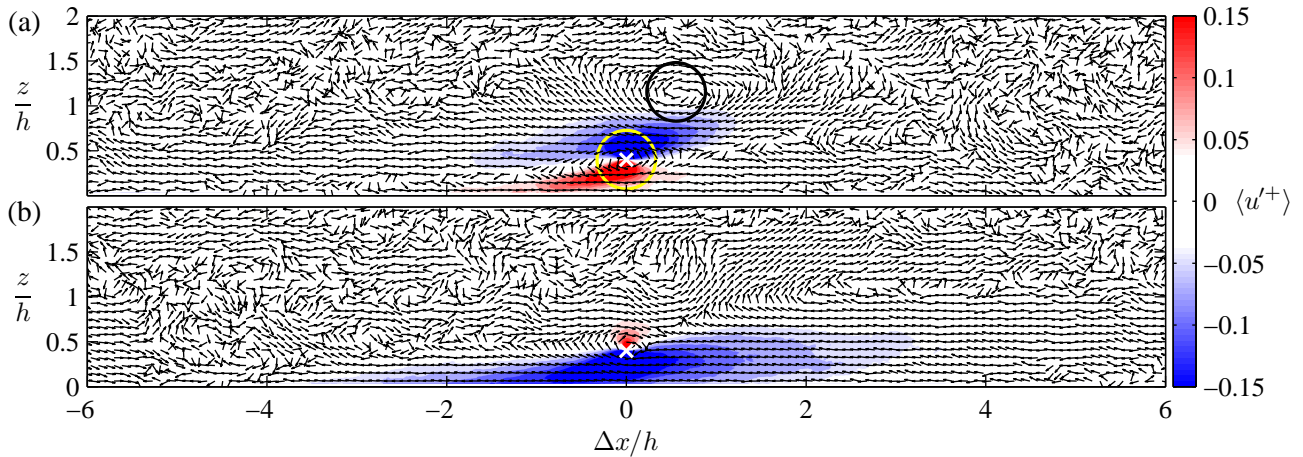

Figure 5: Plots of fluctuating directional fields, conditionally averaged on (a) positively signed and (b) negatively signed swirl events at the reference position of $z = 0.4h$. Δx is the streamwise distance from the condition point. Contour plots in the background show u'^+, conditionally averaged on (a) positively signed (b) negatively signed swirl events at the reference position of $z = 0.4h$. Contour levels indicate (a) $\langle u'^+|\lambda > 0 \rangle$ and (b) $\langle u'^+|\lambda < 0 \rangle$. White '×' indicates the condition points. Yellow and black circles in (a) highlight a pair of counter-rotating vortices. Magnify the online copy for the clearer view.

cal evidence for the wall-to-wall interaction in the channel flow. However, the wall-to-wall influence of small-scale motions near the wall is still in doubt and warrants further investigation.

References

[1] Adrian, R. J. and Moin, P., Stochastic estimation of organized turbulent structure: homogeneous shear flow, *J. Fluid Mech.*, **190**, 1988, 531–559.

[2] Christensen, K. T. and Adrian, R. J., Statistical evidence of hairpin vortex packets in wall turbulence, *J. Fluid Mech.*, **431**, 2001, 433–443.

[3] Dean, R. B. and Bradshaw, P., Measurements of interacting turbulent shear layers in a duct, *J. Fluid Mech.*, **78**, 1976, 641–676.

[4] Hambleton, W. T., Hutchins, N. and Marusic, I., Simultaneous orthogonal-plane particle image velocimetry measurements in a turbulent boundary layer, *J. Fluid Mech.*, **560**, 2006, 53–64.

[5] Monty, J., *Development in smooth wall turbulent duct flows.*, Ph.D. thesis, The University of Melbourne, 2005.

[6] Sabot, J. and Comte-Bellot, G., Intermittency of coherent structures in the core region of fully developed turbulent pipe flow, *J. Fluid Mech.*, **74**, 1976, 767–796.

[7] Teitel, M. and Antonia, R. A., The interaction region of a turbulent duct flow, *Phys. Fluids A*, **2 (5)**, 1990, 808–813.

[8] Wu, Y. and Christensen, K. T., Population trends of spanwise vortices in wall turbulence, *J. Fluid Mech.*, **568**, 2006, 55–76.

[9] Zhou, J., Adrian, R. J., Balachandar, S. and Kendall, T., Mechanisms for generating coherent packets of hairpin vortices in channel flow, *J. Fluid Mech.*, **387**, 1999, 353–396.